UCRL-87088 Rev. 1
PREPRINT
Conf-820801--10

EXPERIMENTAL STUDY OF FLAME PROPAGATION IN SEMICONFINED GEOMETRIES WITH OBSTACLES

P. A. Urtiew, J. Brandeis, and W. J. Hogan

Prepared for presentation at the
19th International Symposium on Combustion,
Haifa, Israel, August 8-13, 1982

February 8, 1982

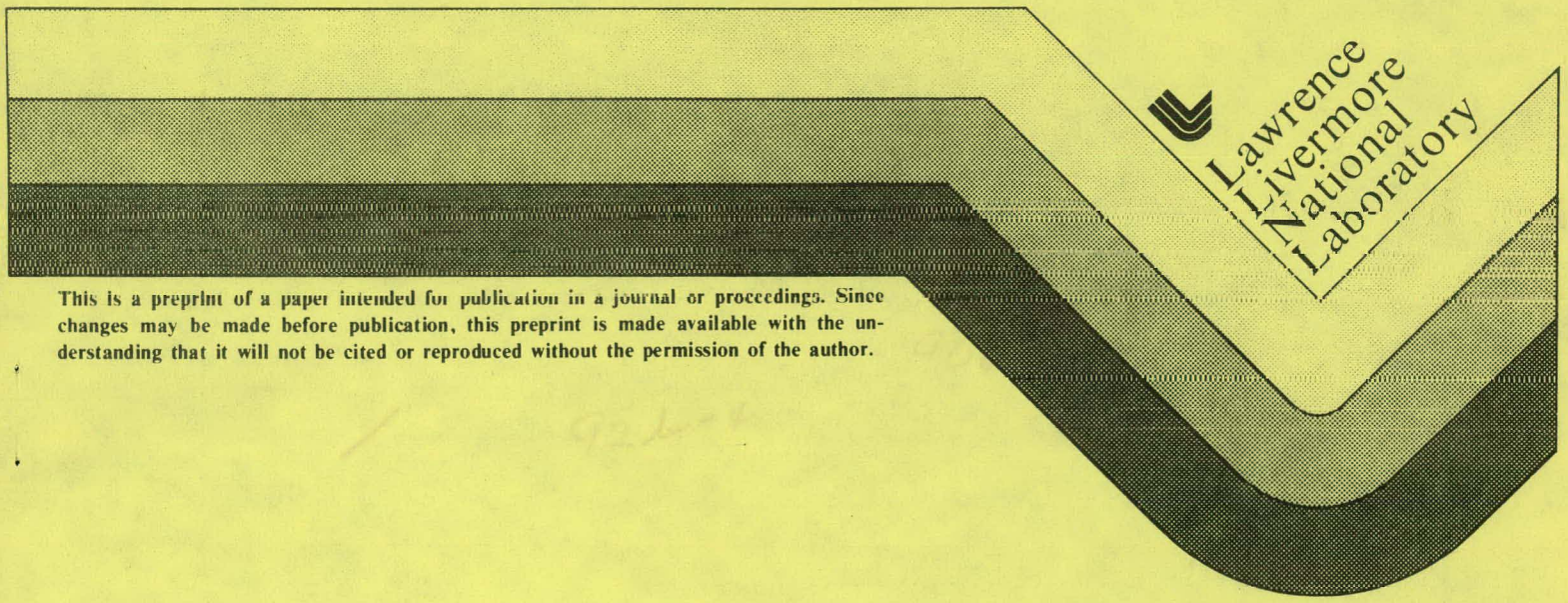

DISCLAIMER

UCRL--87088 Rev. 1

DE82 009407

UCRL-87088 Rev. 1

EXPERIMENTAL STUDY OF FLAME PROPAGATION IN SEMICONFINED GEOMETRIES WITH OBSTACLES

P. A. Urtiew, J. Brandeis, and W. J. Hogan

Lawrence Livermore National Laboratory
Livermore, California 94550

Subject Matter:

(3) Experimental Methods
(21) Structure of Combustion Wave
(32) Turbulent Combustion

MGW

EXPERIMENTAL STUDY OF FLAME PROPAGATION IN SEMICONFINED GEOMETRIES WITH OBSTACLES

P. A. Urtiew, J. Brandeis, and W. J. Hogan

Lawrence Livermore National Laboratory
Livermore, California 94550

ABSTRACT

Accidents in which large quantities of liquefied natural gas (LNG) or other combustible materials are spilled can potentially lead to disastrous consequences, especially if the dispersing combustible cloud finds a suitable ignition source. So far, very little is known about the detailed behavior of a large burning cloud. Full-scale experiments are economically prohibitive, and therefore one must rely on laboratory and field experiments of smaller size, scaling up the results to make predictions about larger spill accidents. In this paper we describe our laboratory-scale experiments with a combustible propane/air mixture in various partially confined geometries. We summarize the experimental results and compare them with calculated results based on numerical simulations of the experiments. Our observations suggest that the geometry of the partial confinement is of primary importance; turbulence-producing obstacles can cause acceleration in the flame front and, more important, can cause a faster burnout of the combustible vapor.

INTRODUCTION

The growing and increasingly interdependent world energy economy requires that liquefied gaseous fuels (LGFs) such as liquefied natural gas and liquefied petroleum gas (LNG and LPG) be transported and stored in ever greater quantities around the world. Modern cryogenic storage and transport technology makes transoceanic movement of natural gas economically feasible, allows transport of LPG and other gaseous fuels by tanker trucks and railcars to locations not accessible by pipeline, and permits peak winter gas demands to be met without oversized pipelines by liquefying the gas at the users' end during the summer and regasifying it during the winter. Economic considerations have led to larger and larger LGF containers. The biggest ships and land-based storage tanks for LNG now contain more than 100,000 m^3 of the liquid.

These factors make it likely that accidental releases of increasingly larger amounts of these materials will become more common. The 1944 Cleveland LNG accident which killed 125 persons involved the release of 2000 m^3 of LNG. The specter of what could happen in an accidental release of many times that amount, combined with the absence of a sound technical understanding of the phenomena that could occur in such an accident, has led to the creation of some very disturbing scenarios. A better understanding of fundamental combustion and detonation phenomena in fuel/air mixtures is badly needed.

Many investigations have been conducted with various ignition sources and fuels in different experimental arrangements to determine when and under what conditions a detonation process can be started and sustained. The general opinion formed in these investigations is that, in an unconfined area without obstacles to cause turbulent eddies, a detonation process cannot be started in a cloud of vaporized LNG in air by a "mild" ignition source. More specifically, Bull et al.[1] state that an ignition source containing less energy than is in a 3-kg charge of tetryl cannot start a detonation in a cloud of air mixed with natural gas containing 10% ethane or propane in methane.

The investigations just mentioned relate to the detonation process. However, devastating levels of overpressure can also be produced by a rapid deflagration and even from an accelerating flame.[2,3] Recently, by applying

the acoustic source theory, Strehlow[4] has suggested that in a nonspherical cloud the overpressure generated by a constant-velocity flame is much smaller than that expected from a one-dimensional (spherical) theory. Computer simulations we have done on nonspherical clouds confirm this prediction. However, there still remains the question of whether or not, in realistic cases, mechanisms exist that can cause an acceleration of the flame.

The purpose of our studies was to examine experimentally various physical effects inherent in the flame propagation process in a semiconfined geometry, and to examine the utility of computer modeling of flame propagation as a tool for predicting flame acceleration in complicated geometries.

EXPERIMENTS

Most of the previous work done with gaseous combustible mixtures has either been in confined geometries (tubes or vessels), to study ignition, flame acceleration, transition to detonation, and properties of the fully developed detonation, or in unconfined geometries, to determine the minimum amount of energy needed to cause a direct initiation of a detonation. Until very recently, semiconfined geometries have not been considered at all, and yet, in real life, accidental spills will most probably occur in dikes, channels, streets, harbors, etc., which are far from either completely confined or unconfined.

Recently, several groups of researchers, besides our own, have started to investigate the problem in semiconfined geometries. Among them are Lee's group at McGill University,[5-8] Strehlow,[9] and Zeeuwen.[10] They are all interested in flame acceleration due to obstacles, with special interest in the effect of fuel compositions[10] and the degree of confinement[8] or turbulence. Our studies are also addressed to the problem of flame propagation over obstacles in a semiconfined geometry, with the main objective being to identify and to model the mechanisms leading to flame acceleration and its associated overpressures for future implementation into large-scale tests.

Our test chamber, illustrated in Fig. 1, is 90 cm long, 30 cm high, and 15 cm wide. It is open on top and at the far end. The sidewalls are made of high-quality glass panels to allow optical observation with a 30.5-cm schlieren system. Metal ribs between individual glass panels serve as holders for ioniz-

ation probes and pressure gauges. A bank of 25 spark plugs is installed in the near end wall to provide the type of ignition desired. A single spark plug can be fired for a point-source ignition, five spark plugs for a line ignition, or even all 25 simultaneously for a plane ignition.

The floor of the test chamber is porous, made of sintered brass, to allow filling the gas from the bottom across the whole horizontal cross section. Under the porous floor there is a plenum chamber, which is filled from a cylinder containing premixed gas, through a safety-designed manifold system. All the tests in this series were carried out with premixed, CO-balanced, propane/air mixtures, i.e., 5.66 vol% propane in air. The height of the cloud is controlled by the height of a drop door at the open end of the chamber (the door is dropped just before firing), or by a removable sliding plate placed at a particular height during the filling procedure and removed just before firing.

To study the effects of turbulence, in some tests we placed obstacles on the floor across the whole width of the chamber. They were either 35 mm or 92 mm high, 19 mm thick, and spaced 9.5 cm apart along the chamber (behind each metal spacer) to allow unobstructed view of the burnout of the gas pockets between obstacles.

DISCUSSION OF RESULTS

To establish the baseline against which we could observe the effect of the obstacles once they were introduced into the flow, we ran a few tests without obstacles. Figure 2 is a plot of the times at which the flame reached various positions down the channel.

The 12-inch (30-cm) schlieren system allowed us to photograph an event through only three windows at a time. Thus, we had to repeat each test at least four times, with nominally the same conditions, to obtain schlieren coverage over the entire chamber. The line shown in Fig. 2 represents the flame path in time as it appeared in the four schlieren photo sequences. One frame of each sequence is shown as an insert. The corresponding time of each photo is indicated by an arrow.

On the time-distance diagram, the slope of the trace represents the velocity of propagation. Thus, in this case, as indicated by the numbers

along the line, the flame propagated through the chamber with a velocity ranging from 2.3 to 3.2 m/s. The initial velocity agrees well with the theoretical expectation of the laminar burn rate as modified by the density ratio across the flame:

$$R_f = \frac{\rho_0}{\rho_1} S_L = 7.5(0.43) \simeq 3.2 \text{ m/s}.$$

Here R_f is the flame speed relative to a stationary observer, ρ_0 and ρ_1 are the density before and after burning, respectively, and S_L is the laminar burning velocity of the mixture. The flame velocity drops when the flame reaches the interface between gas mixture and unconfined air at the top of the chamber.

One interesting observation to be made here pertains to the structure of the flame front and its progressive wrinkling as it continues its propagation away from the ignition source. The first trace of wrinkling is seen in the very first window near the back wall, presumably due to interaction of the flame with the side walls or with the pressure waves generated at the flame front and reflected from the side walls in a nonlinear fashion. Toward the end of the chamber, the flame becomes turbulent in the sense that there is a fine cellular structure on top of a coarse flame that is folding and expanding. At this point, the flame velocity increases slightly again.

Introduction of obstacles into the flow led to higher flame velocities. As mentioned earlier, only two obstacle heights were used in this series of tests, and spacing of the obstacles along the chamber was always kept the same.

Figure 3 shows the effect of obstacles on the flame speed as deduced from the ionization-probe data. The width of the shaded areas qualitatively indicates the degree of reproducibility between various tests.

As evident from this figure, the height of the obstacles did not play a significant role. A larger effect on the initial acceleration was produced by the location of the ignition source, as illustrated in the inserted sketches A and B. In all cases, the ignition was performed with five spark plugs in a horizontal row. Flames ignited by the row of spark plugs next to the floor (B) seemed to accelerate faster to their final velocity than flames ignited by the row of spark plugs higher above the floor (A).

To determine how velocity of the flame changes along its path, the time-distance data retrieved from the ionization probes have been translated into

velocity-distance information. The results, shown in Fig. 4, represent only an average value for each of the four cases, with an error bar indicating the spread between individual tests. What is of interest here is the manner in which each case attains its final flame speed. While corner ignition produces a flame velocity that initially overshoots and then settles back to its apparent final velocity, the elevated ignition source produces a flame velocity that accelerates somewhat slower in the beginning. The final flame velocity, however, for both sizes of obstacles and both igniter positions, does not differ by more than 2 m/s. The presence of obstacles clearly increased the flame velocity from 3 m/s to 5 or 6 m/s, but the additional acceleration occurred within the first cell for most cases, and in no case was continuous acceleration observed. The fact that the location of ignition plays a significant role in the initial flame acceleration makes it rather evident that the initial stages of the process are governed by fluid dynamics phenomena. The pressure waves generated by the flame front reflect back from the obstacle and, depending on the relative height of the obstruction, retard the propagation of the flame front and deform its initial cylindrical shape.

This phenomenon of initial distortion of the flame front and retardation of its progress is illustrated in Fig. 5, which depicts oscillations of the flame front as it travels across the first interval and over the obstacle. In Fig. 5 both sizes of obstacles are represented. The individual frames of the photographic sequence, included as inserts, further illustrate the actual shape of the distorted flame front. Some oscillations of the flame front are carried over into the second interval between the obstacles, because at these velocities the flame front curls down over the obstacle and into the pocket rather than traveling directly along the chamber.

We have also looked into the effect of small gaps under the obstacles. Figure 6 illustrates this effect by showing the time-distance plot of all the ionization-probe data taken with the 92-mm obstacles. Raising all the obstacles 4 mm above the floor produced a dramatic change, giving a flame velocity of about 20 m/s. Eliminating the gap on the first three obstacles lowered the initial velocity to about 6 m/s, as before. However, the gaps left open downstream sometimes caused the flame to accelerate, as evident from a sudden change in the slope of experiments 73, 77, 80, and 81. There was no obvious reason why the flame sometimes accelerated and sometimes did not. The

third group of traces (82, 83, and 84), shown for reference, represents the case of no gaps and ignition source off the floor, as seen in Fig. 4.

Most of the tests conducted so far in our combustion chamber do not show a continuous acceleration of the burning process; however, some of them do, and that may cause concern. Such a continuous acceleration is best visualized in Fig. 7, which represents the plot of velocity vs distance. The flame is shown to cross the first few obstacles at around 5 ± 1 m/s, and then take off to values exceeding 15 m/s. However, since we have not reached the steady 20-m/s value observed by the ionization probes in the raised obstacle case, we cannot conclude that the flame velocity will continue to rise indefinitely.

The reason for a faster burning rate with a gap under the obstacle is illustrated in Fig. 8, which contains two short sequences of schlieren photographs depicting flame propagation with and without the gaps. Without the gaps, the flame leaps over the obstacles at a certain rate, leaving the pockets to burn out at a later time; with gaps, the flame finds another path to enter the next pocket and burn it from the bottom up. Thus, with gaps under the obstacles we are not only dealing with faster flames but also with an increase in the flame surface area, both of which, when combined, lead to a faster burnout of the combustible mixture.

As yet, we have not been able to detect any significant amount of overpressure. However, a decrease in the burnout time, such as that caused by increases of both flame speed and flame surface area, provides the necessary conditions according to Strehlow.[4] His claim is that in the three-dimensional case the overpressure is generated not by the rate of energy release, but rather by the first time derivative of that rate as described by the following expression:

$$\bar{P} \sim \frac{d}{dt} [S_u(t) \cdot A_f(t)] ,$$

where

$$\bar{P} = \frac{P - P_0}{P_0},$$

S_u is the effective normal burning velocity, and A_f is the effective frontal area of the flame. Since our small-scale experiments are not,

strictly speaking, three-dimensional, the effect of energy release rate on overpressure in our case should be more pronounced. The small scale of the experiment and the small amount of combustible mixture prevent us from seeing more of that effect.

MODELING EFFORTS

The numerical simulation of the experiments was carried out by solving the compressible hydrodynamic conservation equations, the heat conduction equations, the equations for transport and diffusion of chemical species, and the chemical kinetics equation. One-step chemistry, together with Arrhenius kinetics, was used to model the chemical reactions. The two-dimensional finite difference analogs of the above-mentioned equations were solved using the TDC computer code described in Ref. 11. The simulations (in general) employed a 96-by-35 computational net, stretched in the vertical direction in order to allow the displacement of the upper (open) boundary by a distance greater than five times the height of the region occupied by the reacting mixture.

Figure 9 shows the numerical results for flame propagation without the obstacles (on a time-distance plot) for both an open chamber and one closed by a lid 15 cm above the floor. The closed geometry was used for the purpose of determining the pre-exponential constant in the Arrhenius law. The computed results for the open geometry lie within the band occupied by the experimental results.

Figure 10 presents the results for flame propagation in an open chamber, with obstacles 92 mm and 35 mm high, evenly spaced along the floor. Computed isotherms representing the shape of the flame front are shown as inserts. Also shown here is the spread of experimental data described earlier in Fig. 3.

As one can note, the computed results fall right between the two groups of experimental data. The effect of ignition location as computed is less pronounced than that observed during the experiments. Furthermore, the computed results show that the initial flame is faster when ignited at midheight of the obstacles, although the experiments indicate the opposite. Obstacle size seems to have a slightly greater effect on initial flame acceleration in the computed results than in the experiments. In the computer simulations, most

of the changes affecting the flame front seem to occur at the very beginning, ahead of the first obstacle, showing features of flame distortion and acceleration similar to those observed in the experiments; but once the first obstacle is cleared, the computed results for both 92-mm-obstacle cases tend to converge to the results for the no-obstacle case. The computed results for the 35-mm-obstacle case show that it takes two obstacles to accelerate the flame before stabilizing it at a new higher velocity. Thus, unlike the experiments, the computer simulation does not indicate a great increase of the final velocity due to the presence of the obstacles. Yet the simulation correctly predicts (qualitatively) most of the observed features associated with flame propagation. We are led to conclude that the primary mechanism by which obstacles accelerate a flame is by changing the turbulence structure of the flow, a mechanism which has not been incorporated into the model. The turbulence structure may also be influenced (especially in the vicinity of obstacles) by the three-dimensionality of the actual flow, which is ignored in the two-dimensional numerical model.

SUMMARY AND CONCLUSION

We have briefly reviewed our experimental and computational efforts and demonstrated the effect of obstacles on flame propagation in a semiconfined combustion chamber. We have demonstrated that obstacles can increase the speed of flame propagation, and that if the obstacles are slightly raised they cause a quicker burnout of the medium and faster flame travel even with incomplete confinement. In some cases we have seen the speed of the flame and burnout change during the process if the flame front encounters a different configuration of obstacles. We cannot explain why the flame accelerated in some cases but not in others having nominally the same configuration.

The numerical model was able to predict many of the features observed in the experiments. The computed results, however, did not always show that an overall increase in the flame velocity is caused by the obstacles. We conclude that the obstacles must accelerate the flame primarily through changing its turbulence structure. This aspect of the problem is, for the time being, beyond the capabilities of our predictive methods.

The ultimate aim of our efforts is to identify the various factors affecting flame acceleration processes, interpret their effects, and incorporate them into computational models that will give us a predictive capability for larger and more complicated cases. Small-scale experiments followed by intermediate-scale field tests will provide the necessary input for attaining this goal.

ACKNOWLEDGMENTS

We are grateful to D. J. Bergmann for his excellent assistance with the computational efforts. This work was performed under the auspices of the U.S. Department of Energy by the Lawrence Livermore National Laboratory under contract number W-7405-Eng-48.

REFERENCES

1. Bull, D. C., Elsworth, J. E., and Hooper, G.: Combustion and Flame 34, 327 (1979).
2. Kuhl, A. L., Kamel, M. M., and Oppenheim, A. K.: Fourteenth Symposium (International) on Combustion, p. 1201, The Combustion Institute, 1973.
3. Strehlow, R. A., and Baker, W. E.: The Characterization and Evaluation of Accidental Explosions, NASA CR 134779 AAE 75-3. Prepared for Aerospace Safety Research and Data Institute, Lewis Research Center, Cleveland, Ohio, 1975.
4. Strehlow, R. A.: The Blast Wave from Deflagrative Explosions: An Acoustic Approach, paper presented at the Fourteenth Loss Prevention Symposium of AIChE, Philadelphia, Pa., June 1980.
5. Moen, I. O., Donato, M., Knystautas, R., and Lee, J. H.: Flame Acceleration Due to Turbulence Produced by Obstacles, McGill University, Montreal, Canada, preprint, 1979.
6. Moen, I. O., Donato, M., Knystautas, R., Lee, J. H., and Wagner, H. Gg.: Progress in AIAA Astronautics and Aeronautics 75, 33 (1981). Proceedings of the Seventh International Colloquium on Gas Dynamics of Explosions and Reactive Systems.

7. Chan, C. S., Lee, J. H., Moen, I. O., and Thibault, P.: "Turbulent Flame Acceleration and Pressure Development in Tubes," McGill University, Montreal, Canada, private communication, 1980.
8. Chan, C. S.: private communication, 1981.
9. Strehlow, R. A.: private communication, 1981.
10. Zeeuwen, J. P.: private communication, 1981.
11. Haselman, L. C.: TDC--A Computer Code for Calculating Chemically Reacting Hydrodynamic Flows in Two Dimensions, Lawrence Livermore National Laboratory, UCRL-52931, May 1980.

FIGURE CAPTIONS

Fig. 1. Semiconfined test chamber for optical combustion experiments.

Fig. 2. Time-distance diagram of the burning process without obstacles. Inserts represent schlieren photographs of the flame taken during four different experiments. Numbers along the curve indicate flame velocities (m/s).

Fig. 3. Time-distance plot of ionization-probe data taken during experiments with obstacles.

Fig. 4. Velocity-distance plot deduced from ionization probe data shown in Fig. 3.

Fig. 5. Time-distance plot of flame propagation through the first 30 cm of the test chamber fitted with obstacles. The flame path is deduced from the sequence of schlieren records.

Fig. 6. Time-distance plot of all ionization-probe data taken with 92-mm obstacles in the chamber. Curves are labeled by shot number.

Fig. 7. Velocity-distance plot showing continuous acceleration of the burning process during some of the tests.

Fig. 8. Two sequences of schlieren records taken with 92-mm obstacles in the chamber: (a) No gaps under the obstacles, 2.17 ms between frames. (b) Gaps 4 mm high under the obstacles, 1.09 ms between frames.

Fig. 9. Time-distance plot of the computed flame propagation through open and closed channels without obstacles. Solid lines represent computed results. Points and error bars indicate experimental data.

Fig. 10. Time-distance plot of the computed flame propagation through the open channel with obstacles 35 and 92 mm high. Computer output of the flame profile is included as inserts.

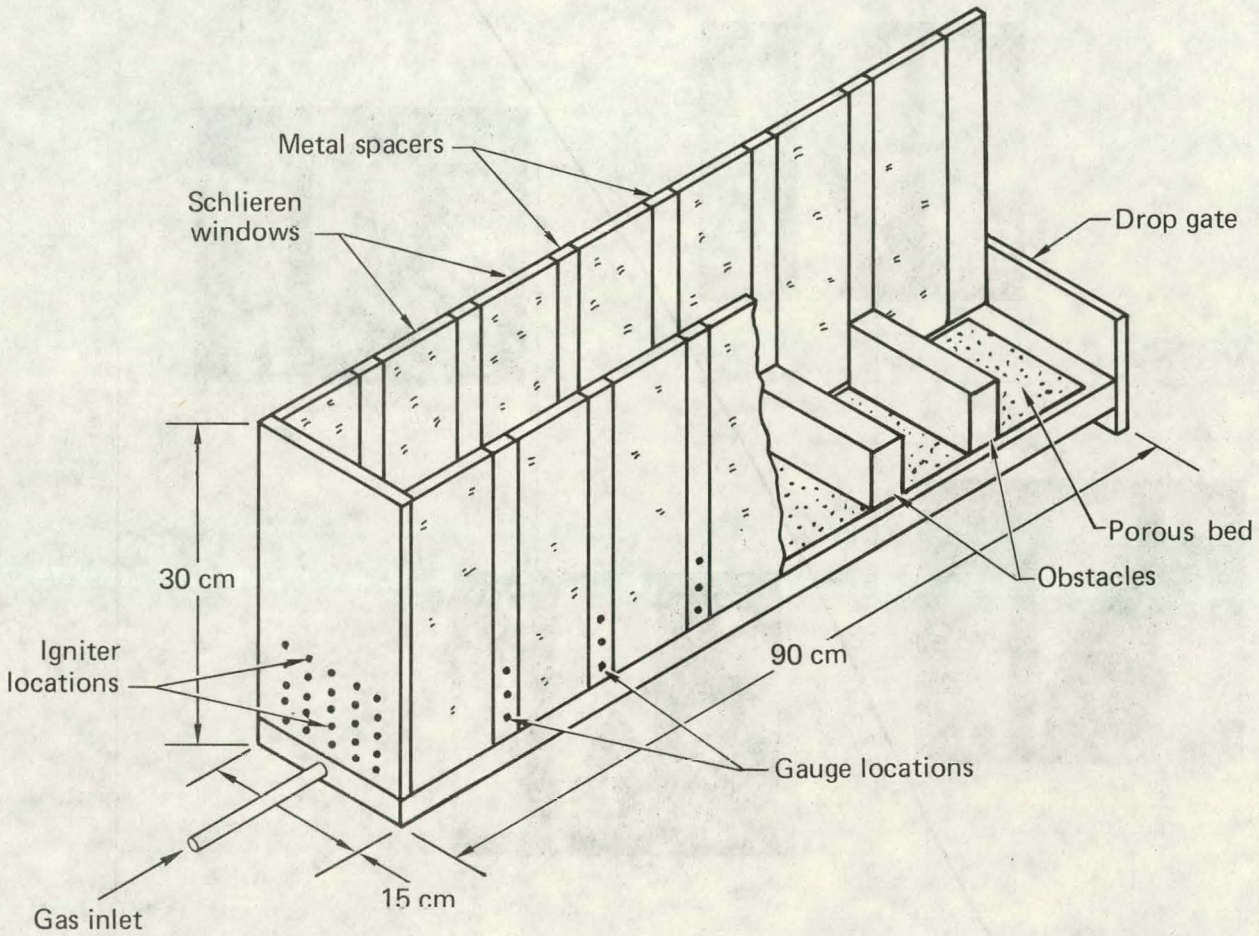
Metal spacers
Schlieren windows
Drop gate
Porous bed
Obstacles
30 cm
Igniter locations
90 cm
Gauge locations
15 cm
Gas inlet

Fig. 1. - Urtiew

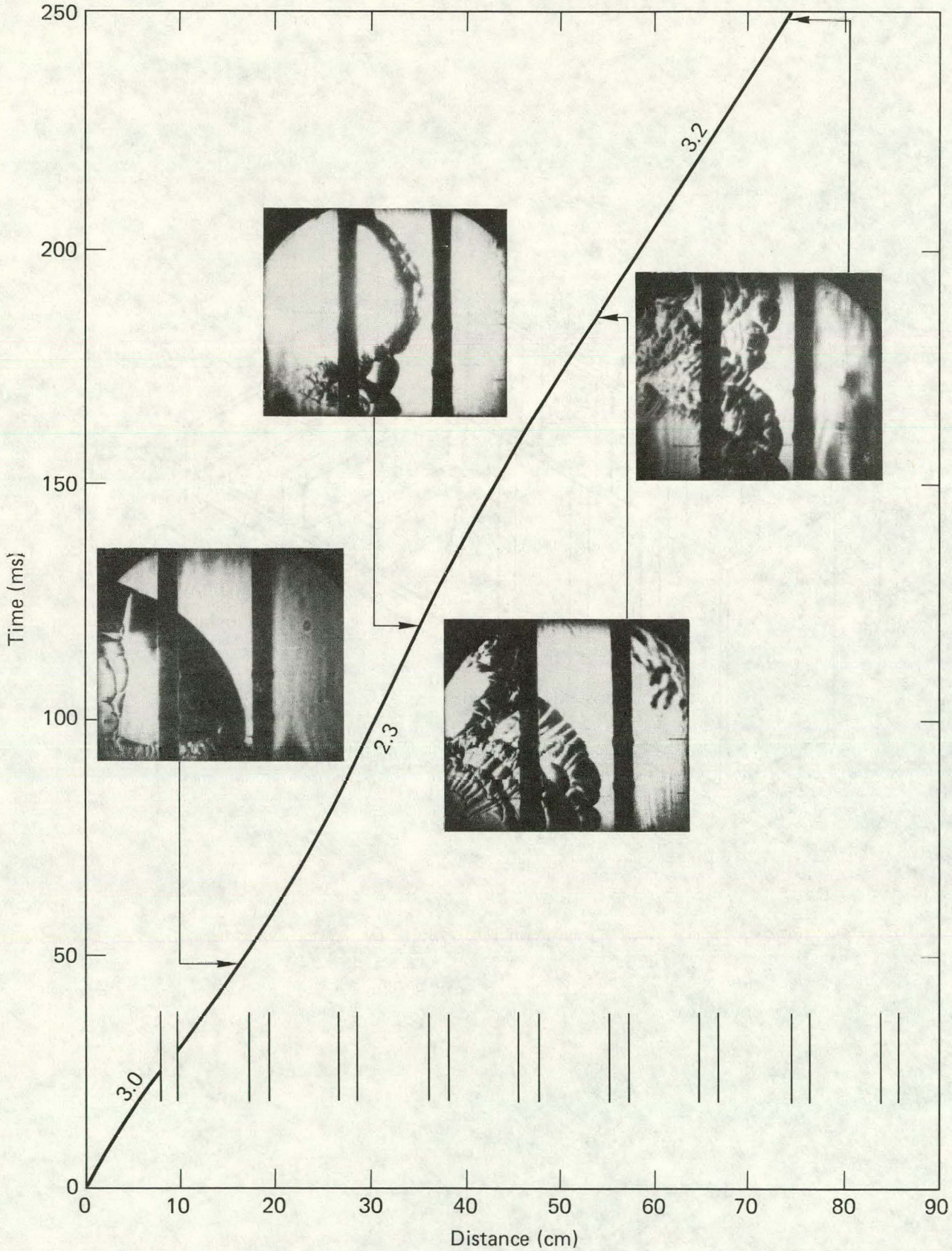
250
200
150
100
50
0
Time (ms)
0
10
20
30
40
50
60
70
80
90
Distance (cm)
3.0
2.3
3.2

Fig. 2. - Urtiew

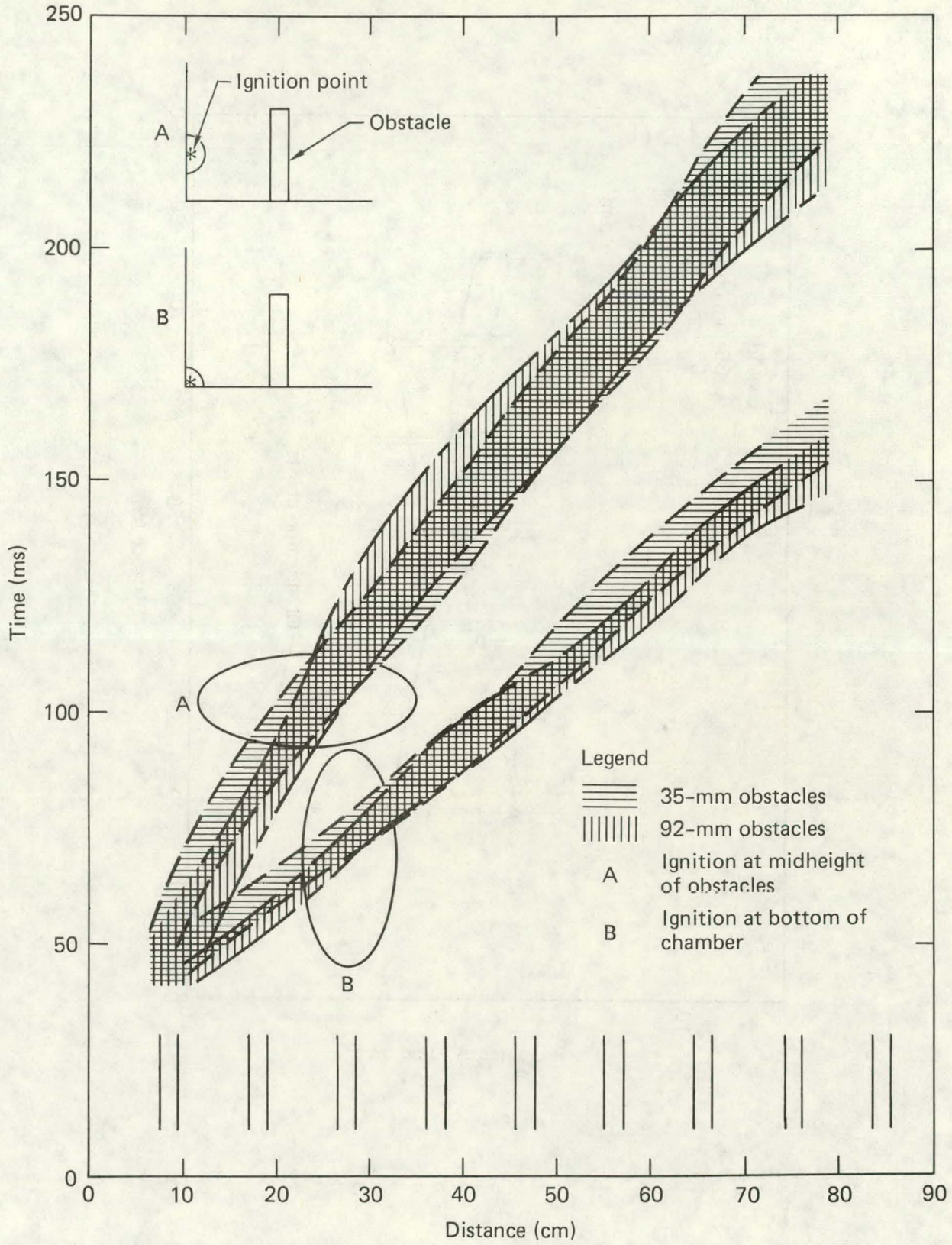
250
200
150
100
50
0
Time (ms)
Ignition point
Obstacle
A
B
A
B
Legend
35-mm obstacles
92-mm obstacles
A
Ignition at midheight of obstacles
B
Ignition at bottom of chamber
0
10
20
30
40
50
60
70
80
90
Distance (cm)

Fig. 3. - Urtiew

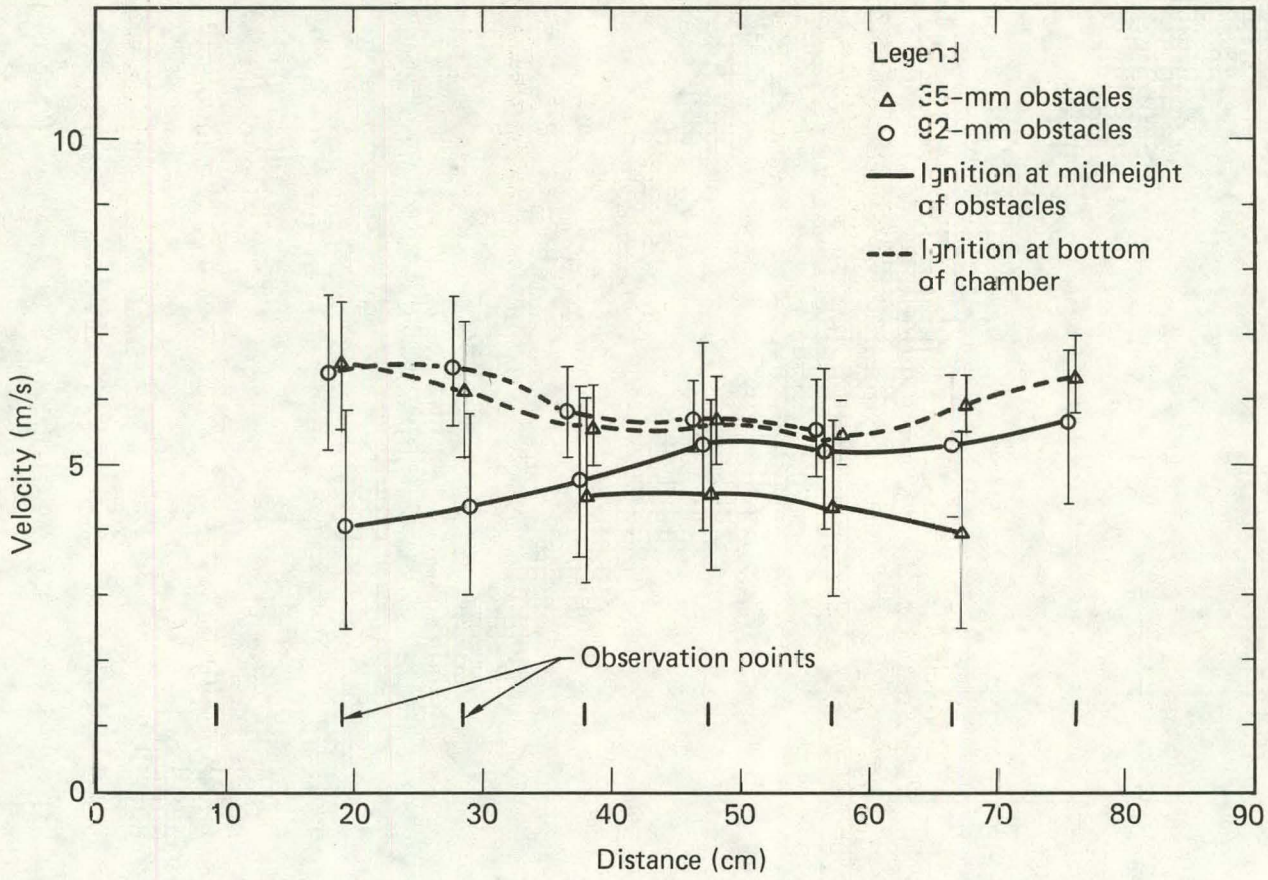
Legend
35-mm obstacles
92-mm obstacles
Ignition at midheight of obstacles
Ignition at bottom of chamber
Observation points
Velocity (m/s)
Distance (cm)
0
5
10
0
10
20
30
40
50
60
70
80
90

Fig. 4. - Urtiew

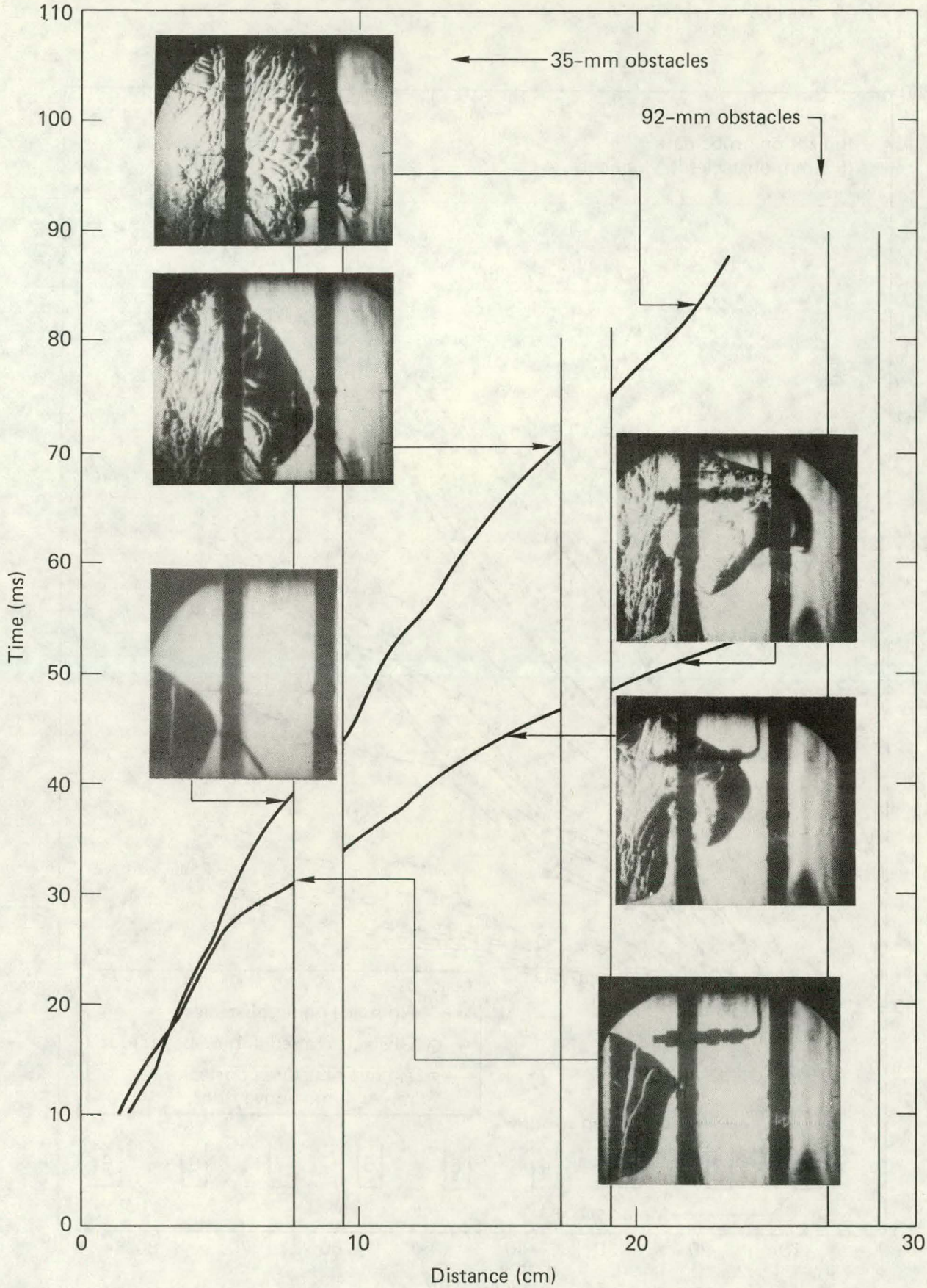
35-mm obstacles
92-mm obstacles
Time (ms)
Distance (cm)
0
10
20
30
40
50
60
70
80
90
100
110

Fig. 5. - Urtiew

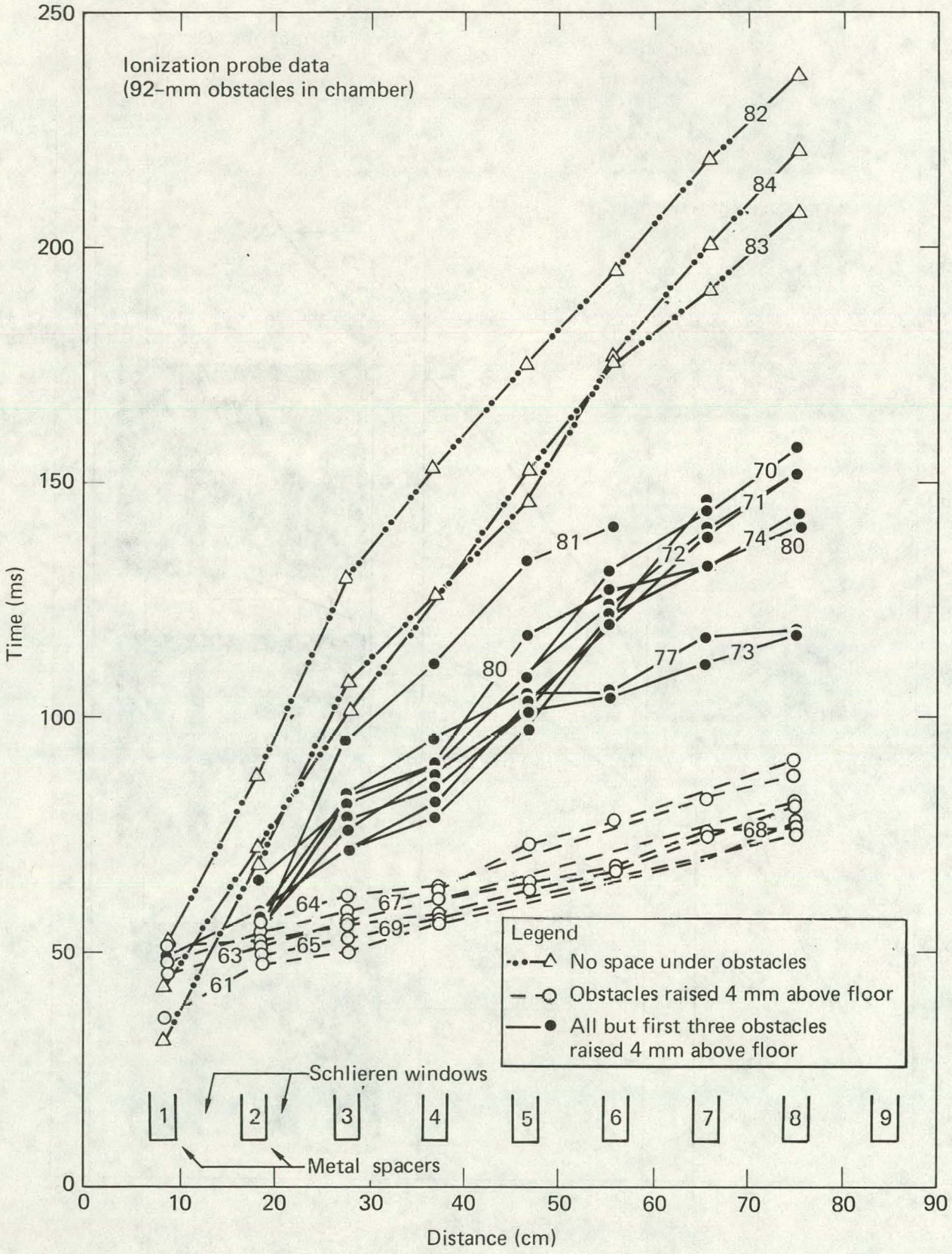
Ionization probe data
(92-mm obstacles in chamber)
Time (ms)
Distance (cm)
250
200
150
100
50
0
0
10
20
30
40
50
60
70
80
90
82
84
83
70
71
74
80
81
72
80
77
73
68
64
67
69
63
65
61
Legend
No space under obstacles
Obstacles raised 4 mm above floor
All but first three obstacles raised 4 mm above floor
Schlieren windows
Metal spacers
1
2
3
4
5
6
7
8
9

Fig. 6. - Urtiew

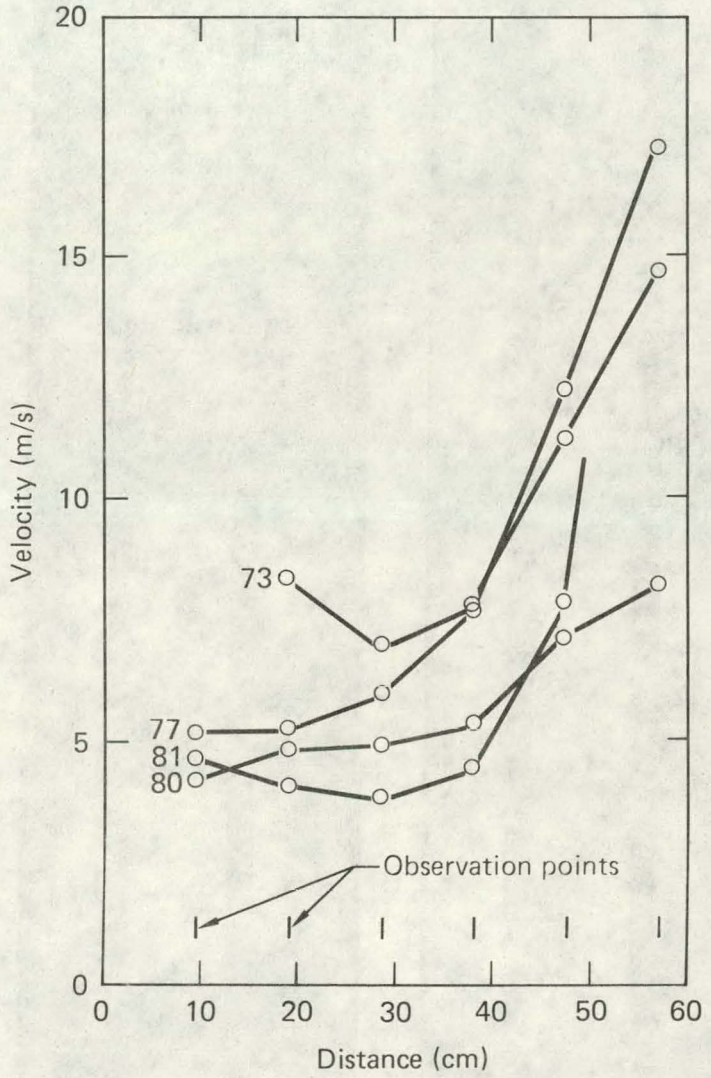
20
15
10
5
0
Velocity (m/s)
73
77
81
80
Observation points
0
10
20
30
40
50
60
Distance (cm)

Fig. 7. - Urtiew

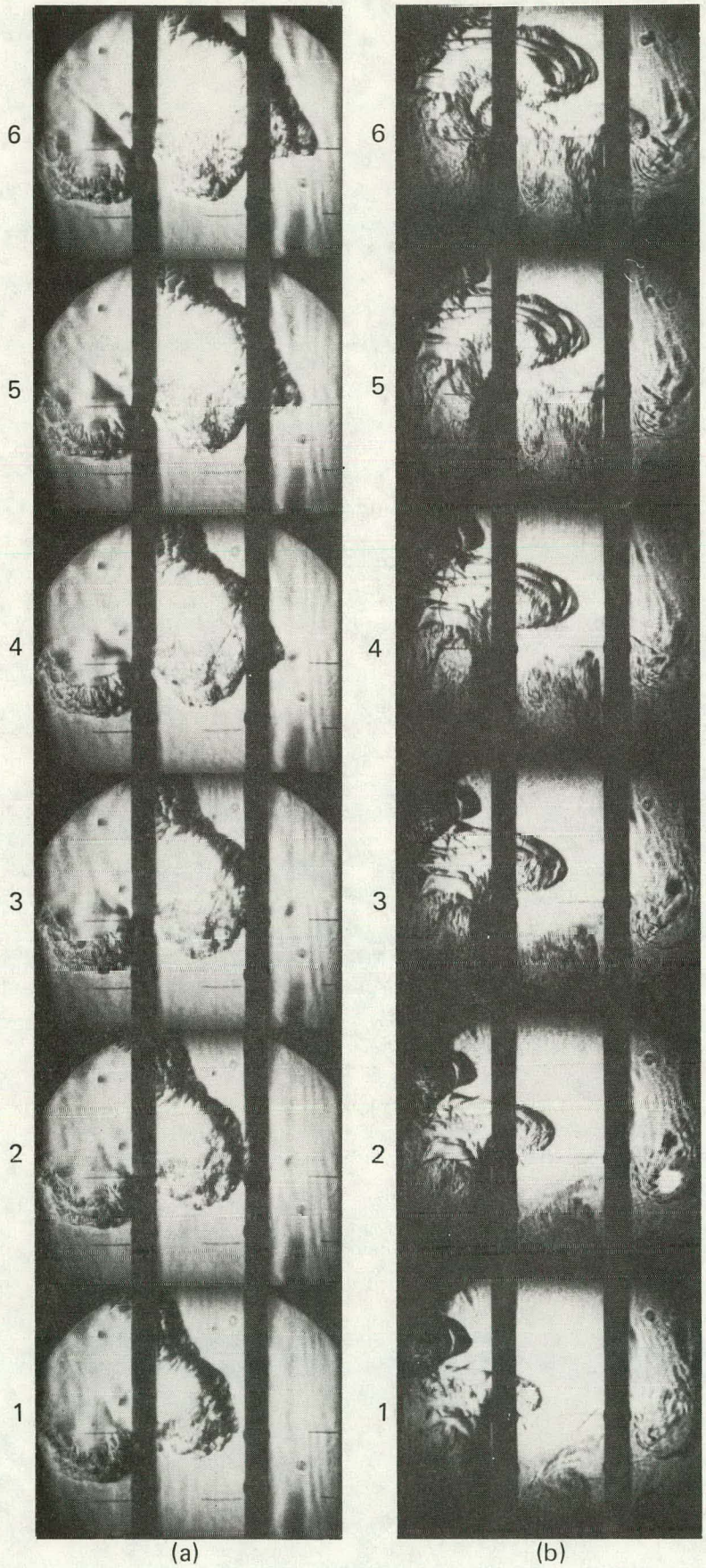

Fig. 8. - Urtiew

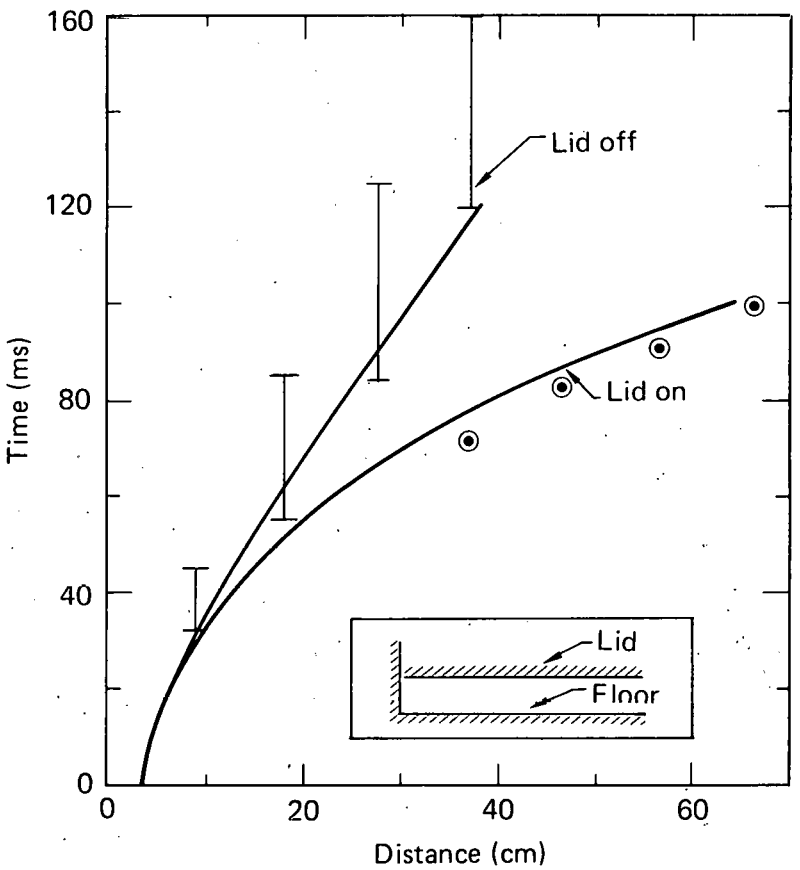
160
120
80
40
0
Time (ms)
0
20
40
60
Distance (cm)
Lid off
Lid on
Lid
Floor

Fig. 9. - Urtiew

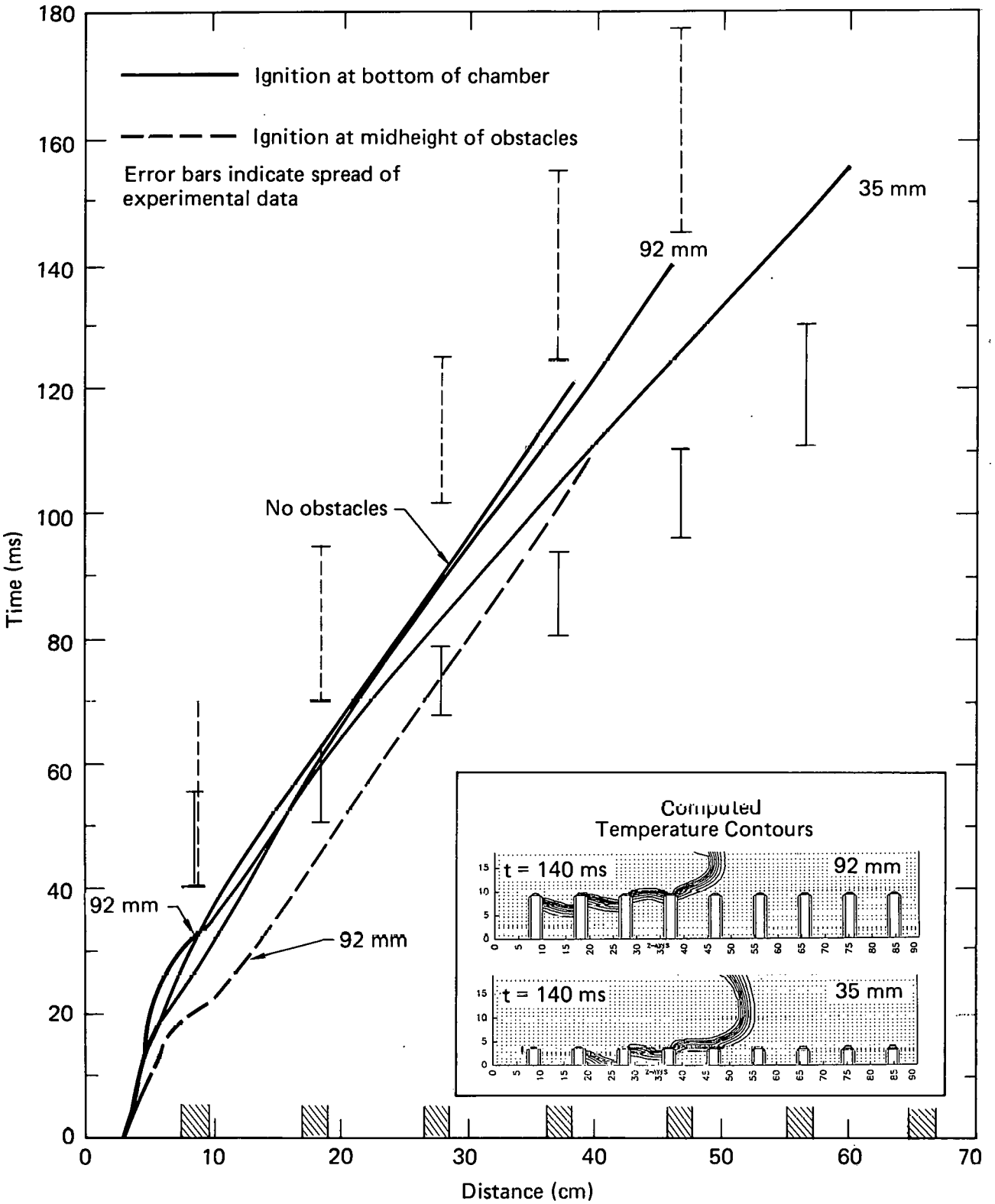

Fig. 10. - Urtiew

Technical Information Department · Lawrence Livermore Laboratory
University of California · Livermore, California 94550